LANGMUIR Article
Cite This: Langmuir 2019, 35, 2989−2996
pubs.acs.org/Langmuir

Pinning-Free Evaporation of Sessile Droplets of Water from Solid Surfaces

Steven Armstrong, Glen McHale,* Rodrigo Ledesma-Aguilar, and Gary G. Wells

Smart Materials & Surfaces Laboratory, Faculty of Engineering & Environment, Northumbria University, Newcastle upon Tyne NE1 8ST, U.K.

ABSTRACT: Contact-line pinning is a fundamental limitation to the motion of contact lines of liquids on solid surfaces. When a sessile droplet evaporates, contact-line pinning typically results in either a stick−slip evaporation mode, where the contact line pins and depins from the surface in an uncontrolled manner, or a constant contact-area mode with a pinned contact line. Pinning prevents the observation of the quasi-equilibrium constant contact-angle mode of evaporation, which has never been observed for sessile droplets of water directly resting on a smooth, nontextured, solid surface. Here, we report the evaporation of a sessile droplet from a flat glass substrate treated with a smooth, slippery, omniphobic covalently attached liquid-like coating. Our characterization of the surfaces shows high contact line mobility with an extremely low contact-angle hysteresis of ∼1° and reveals a step change in the value of the contact angle from 101° to 105° between a relative humidity (RH) of 30 and 40%, in a manner reminiscent of the transition observed in a type V adsorption isotherm. We observe the evaporation of small sessile droplets in a chamber held at a constant temperature, $T = (25.0 \pm 0.1)$ °C and at constant RH across the range RH = 10−70%. In all cases, a constant contact-angle mode of evaporation is observed for most of the evaporation time. Furthermore, we analyze the evaporation sequences using the Picknett and Bexon ideal constant contact-angle mode for diffusion-limited evaporation. The resulting estimate for the diffusion coefficient, D_E, of water vapor in air of $D_E = (2.44 \pm 0.48) \times 10^{-5}$ m^2 s^{-1} is accurate to within 2% of the value reported in the literature, thus validating the constant contact-angle mode of the diffusion-limited evaporation model.

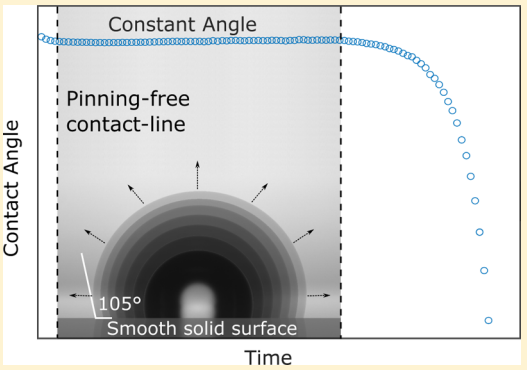

1. INTRODUCTION

Evaporation of liquids occurs when the atmosphere surrounding the liquid is not saturated with the vapor of the liquid.[1] It is a widely observed natural phenomenon and is important for many applications, including inkjet printing,[2] fuel delivery,[3] and heat exchange.[4] In these applications, droplets rest on a solid surface and this introduces two fundamental differences as to how evaporation occurs compared to spherical droplets in free space far from any surface. First, the spherical symmetry for diffusion of vapor into the space around the droplet is broken by the presence of the surface. Second, droplet contact with a surface introduces contact-line pinning, which can be problematic, for example, causing nonuniform deposition of colloidal particles as in the well-known formation of coffee-ring stains.[5] Nonuniform particle deposition causes problems in a diverse range of applications, from nonuniform delivery of the active components in aerosols used in pesticides to nonuniform fluorescence in spotted microarrays.[1,5−8] While, the effect on diffusion of a surface can be modeled, contact-line pinning is usually an unavoidable consequence of the contact between a droplet and the surface to which it is attached.

When a droplet is in contact with a solid surface, and at thermodynamic equilibrium, the contact angle that the droplet makes with the surface, θ_e, in principle, is determined by the interfacial tension of the three interfaces as described by Young's law[9]

$$\cos\theta_e = \frac{\gamma_{SV} - \gamma_{SL}}{\gamma_{LV}} \quad (1)$$

where γ_{SV} is the solid−vapor interfacial tension, γ_{SL} is the solid−liquid interfacial tension, and γ_{LV} is the liquid−vapor interfacial tension. When a droplet is small compared to its capillary length $\kappa^{-1} = (\gamma_{LV}/\rho g)^{1/2}$, where ρ is the density of the liquid and $g = 9.81$ m s^{-2}, it adopts an axisymmetric spherical cap shape when the surface is flat and smooth with no contact-line pinning. However, in practice, contact-line pinning has always been observed to some extent. Picknett and Bexon provided an analytical model describing the ideal case of diffusion-limited evaporation of a sessile droplet in the absence of gravity.[10] Their analysis includes two ideal modes of evaporation.[10] The first corresponds to a constant contact radius (CCR) mode, where the apparent contact angle decreases during evaporation. Because the CCR mode of evaporation requires complete pinning of the contact line, it

Received: November 15, 2018
Revised: January 28, 2019
Published: January 31, 2019

DOI: 10.1021/acs.langmuir.8b03849
Langmuir 2019, 35, 2989−2996

can be achieved experimentally and has been widely studied.[1] The second mode is a constant contact angle (CCA) mode evaporation, where the contact angle is expected to retain a constant value approximating the contact angle predicted by Young's law, while the square of the base radius of the droplet decreases linearly in time.

The observation of the CCA mode evaporation on a smooth (nontextured) flat solid surface remains elusive because it requires complete mobility of the contact line, and the roughness of ordinary flat solid surfaces always results in some contact-line pinning. Contact-line pinning is quantified experimentally by the so-called contact-angle hysteresis: the difference between the advancing and receding contact angles of the droplet. Instead, many experimental studies have reported a stick−slip mode of evaporation, whereby the droplet's contact line is repeatedly pinned until the force from the out-of-equilibrium contact angle increases sufficiently and a depinning event and rapid contact-line motion occurs. Stauber et al. have also detailed another mode of evaporation known as the stick−slide mode of evaporation, where the contact line and contact angle decrease at the same time. They provide a model to predict the lifetime of evaporating drops in stick−slide mode evaporation.[11] Recent comprehensive reviews of sessile drop evaporation are given by Erbil,[1] Cazabat and Guéna,[12] and Larson.[13]

Attempts to experimentally observe the CCA mode of evaporation have included the use of superhydrophobic surfaces and slippery liquid-infused porous surfaces (SLIPS), sometimes referred to as liquid-infused surfaces.[14,15] Superhydrophobic surfaces take advantage of surface texture to suspend droplets in a Cassie−Baxter state[16] on a small solid surface fraction, thereby reducing the droplet−solid contact area, increasing its contact angle and reducing contact-angle hysteresis.[17−19] McHale et al.[20] reported the first experiments of this type using SU-8 textured surfaces with water droplets initially evaporating in CCR mode evaporation, before retreating in a step-wise fashion as the droplet jumps between micropillars and ultimately converting into a Wenzel state, where the droplet is impaled in the texture with a completely pinned contact line.[21] Since then, many works studying evaporation on super hydrophobic surfaces and the effect of contact angle hysteresis has been reported.[22−27] In all of these studies, the surface is no longer smooth but is textured or rough and hydrophobic, with a contact angle far from the value given by Young's law for a smooth nontextured solid surface.

A second approach to observing a CCA mode of evaporation was introduced by Guan et al. who used a SLIPS approach, with a lubricant oil impregnated into a hydrophobic SU-8 textured surface.[28] The lubricant oil completely coats the solid and is immiscible to water, therefore, is not displaced by it. SLIPS enable droplets to slide at tilt angles of less than 1°. However, the high mobility of droplets on SLIPS arises by the replacement of the droplet−solid interface by a droplet−lubricant interface and the removal of all direct contact between the droplet and the solid. On SLIPS, contact angles and contact radii have to be interpreted as apparent contact angles and apparent contact radii from the change in slope of the droplet close to the surface. Guan et al. were able to observe the pinning-free evaporation of water droplets on SLIPS and interpret their evaporation using the Picknett and Bexon diffusion-limited model, modified for the presence of a wetting ridge of the impregnated oil, which surrounds the droplet's base.[28] Ultimately, neither of these two approaches have provided observation of the evaporation of sessile droplets on flat smooth (nontextured) solid surfaces without contact-line pinning. A key challenge remains the ability to remove contact-line pinning during evaporation of sessile droplets from nontextured solid surfaces.

Recently, Wang and McCarthy have reported a method to create slippery omniphobic covalently attached liquid-like (SOCAL) surfaces with contact-angle hysteresis less than 1°.[29] SOCAL surfaces use polydimethylsiloxane (PDMS) chains grafted to the substrate. The chains are flexible and have the ability to move independently of each other. This flexibility results in a completely mobile contact line on the solid that enables droplets to move across a surface with virtually no pinning. Importantly, SOCAL is a covalently attached layer, rather than a liquid coating retained by a surface texture as occurs in SLIPS. It also provides a coating that is on the nanometric scale as opposed to the micrometric scale of SLIPS, allowing for a clearly defined contact angle for a sessile droplet on the coated flat smooth solid surface. The report by Wang and McCarthy of smooth low-hysteresis surfaces via a liquid-like coating with advancing and receding water contact angles of θ_A = 104.6° and θ_R = 103.6° and tilt angles for motion of 4.7° and 1.3° for droplet volumes of 3 and 20 μL, respectively,[29] has been noted by a range of researchers, but few have implemented the method. Jin et al. reported SOCAL contact angles of θ_A = 103.0° and θ_R = 98.2° on silicon substrates[30] and Mizutani et al. have reported grafting SOCAL to surgical diamond wheels for minimally invasive bone surgery, and they also grafted SOCAL to a nickel substrate with a static contact angle θ_s = 94.1° and a sliding angle of 40°.[31] Daniel et al. also reported dissipative force acting on a droplet moving on several types of low-hysteresis surfaces, including a SOCAL surface (prepared following the Wang and McCarthy method) with a minimum critical tilt angle between 5° and 15° to move a 10 μL water droplet but with no values reported for their advancing or receding contact angles.[32]

Here, we report experiments of the evaporation of sessile droplets of water on SOCAL-coated glass surfaces with contact-angle hysteresis of less than 1° over a wide range of relative humidity (RH, from 10 to 70%). In Section 2.1, we describe preparation of SOCAL coatings with highly reproducible contact angles ∼101°−105° and low contact-angle hysteresis $\Delta\theta_{CAH} \approx 1°$. In Section 3, we report data showing the CCA mode evaporation for small sessile water droplets; we consistently measure contact angles close to the static values, and within the bounds expected from the measured and extremely low contact-angle hysteresis. In Section 4, we discuss the entire evaporation sequence including a step change in the observed value of the CCA that occurs at RH between 30 and 40%. Finally, we use the Picknett and Bexon model to analyze the evaporation of individual droplets and provide a set of estimates of the diffusion coefficient. By comparing the evaporation rate to the RH across all experiments, we obtain a second estimate of the diffusion coefficient. Both types of estimate are within 2% of the literature value and show how SOCAL surfaces, which are omniphobic, provide a simple but accurate methodology to determine the diffusion coefficient of volatile liquids.

2. EXPERIMENTAL METHOD

2.1. SOCAL Preparation. SOCAL surfaces were created on 25 × 75 mm glass slides, using the method detailed by Wang and McCarthy, adapted to our specific equipment and with process

DOI: 10.1021/acs.langmuir.8b03849
Langmuir 2019, 35, 2989−2996

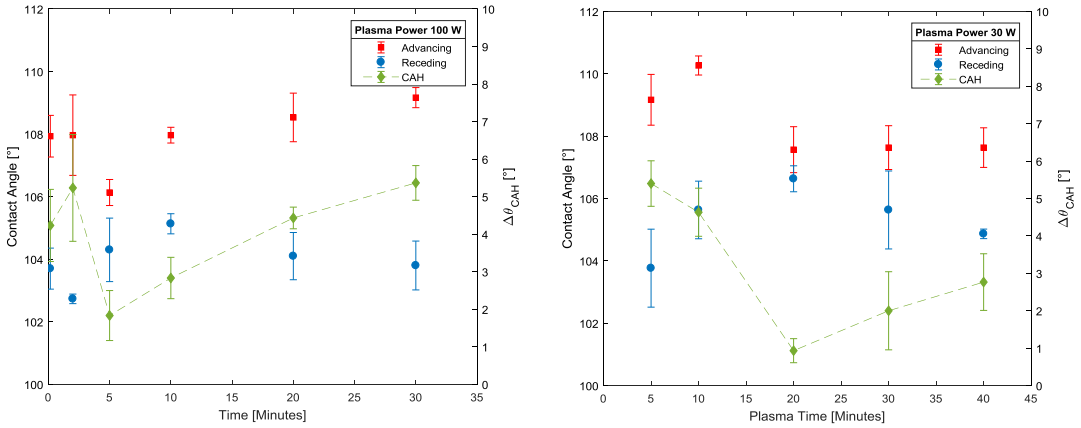

Figure 1. Contact-angle hysteresis ($\Delta\theta_{CAH}$) as a function of plasma time. (Left) shows $\Delta\theta_{CAH}$ as a function of time for 100 W plasma power. (Right) shows $\Delta\theta_{CAH}$ as a function of time for 30 W. The green dashed line is a guide to the eye.

parameters iteratively developed until a reproducible and low contact-angle hysteresis method was achieved.[29] Our optimized method used clean glass slides placed into a Henniker plasma cleaner (HPT-100) at 30% power for 20 min. This step adds OH bonds to the surface. The slide was then dipped into a reactive solution of isopropanol, dimethyldimethoxysilane, and sulphuric acid (90, 9, and 1% wt) for 5 s, and then slowly withdrawn. The slides were then placed in a bespoke humidity-controlled environment at 60% RH and 25 °C for 20 min. During this step, an acid-catalyzed graft polycondensation of dimethyldimethoxysilane creates a homogeneous layer of PDMS grafted to the surface. Unreacted material was then rinsed away with deionized (DI) water, isopropanol, and toluene.

We found that to reliably produce SOCAL surfaces with low contact-angle hysteresis, the following parameters need to be carefully controlled and optimized: plasma exposure time; the RH at which the reaction takes place and the reaction time. With the plasma cleaner set to 100 W power and varying the treatment duration from 30 s to 30 min, we found a minimum in the contact-angle hysteresis occurs at 5 min plasma time ($\Delta\theta_{CAH}$ = 1.8 ± 0.7°). Although very low, this contact-angle hysteresis is larger than previously reported by Wang and McCarthy.[29] By reducing the plasma power to 30 W, we were able to reduce the time sensitivity and achieve $\Delta\theta_{CAH}$ = (0.9 ± 0.3°) with 20 min plasma cleaning time (Figure 1). To assess the reproducibility and the uniformity of results across a surface, the contact-angle hysteresis for each change in the process parameter was assessed using advancing and receding contact-angle measurements taken at three different locations on the surface; the average of the results across all the three locations is reported with its standard deviation.

2.2. Contact-Angle Measurements. Contact-angle measurements of droplets of water on the SOCAL surfaces were carried out using a Krüss drop shape analyzer (DSA 30) and Krüss DSA4 software. A 4 μL droplet of DI water was dispensed onto the surface at room temperature (20−25 °C). A video sequence at 5 frames per s captured the inflation and deflation of the droplet to determine advancing and receding contact angles. The droplet was inflated by 2 μL at 20 μL/min, left to stabilize for 5 s, and then, 2 μL was withdrawn at 1 μL/min. A slow withdrawal speed was used for contact-angle hysteresis measurements to limit the risk that the measured angles were dynamic angles. In all reported measurements, the advancing angle, θ_A, is the angle immediately before the droplet radius begins to increase. Similarly, the receding angle, θ_R, is the angle immediately before the droplet radius begins to decrease. Each reported contact-angle hysteresis value, $\Delta\theta_{CAH} = (\theta_A - \theta_R)$, is the average of contact-angle hysteresis values measured at three different locations on the SOCAL-treated glass slide.

2.3. Evaporation Experimental Procedure. Small (4.0 ± 0.3 μL) droplets of room-temperature DI water (type III, purified in an Elga PURELAB Option-Q lab water purification system) were deposited on a SOCAL-treated glass slide, in a commercial humidity and temperature-controlled chamber (TC30) that had been equilibrated at (25 ± 0.1) °C, attached to a Krüss (DSA 25). The evaporation of the droplets was observed for a range of RH from 10 to 70% (±0.5%) in intervals of 10%. A further sequence of evaporation experiments refined the RH range between 30 and 40% in steps of 2%. The evolution of the contact angle and the contact radius as a function of time were recorded using a Krüss drop shape analyzer (DSA 25), with time-lapse image capture at 10 s intervals (Figure 2). The data and images for each evaporation sequence were analyzed individually to verify the absence of contact-line pinning.

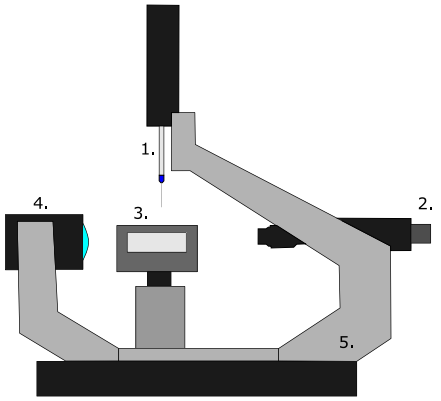

Figure 2. Diagram of experimental setup for evaporation. (1) Automatic syringe dosing unit. (2) Camera with macro lens and barrel. (3) Humidity and temperature-controlled chamber (TC30). (4) Light-emitting diode backlight. (5) Krüss DSA 25.

The contact radius was calculated by identifying the contact base line using the eye; the Krüss Advance software package then tracks the drop radius throughout the evaporation. The contact angle was evaluated using an elliptical fit in the Krüss Advance software, which uses the tangent of the ellipse intersecting the contact base line. This gives a mean contact angle from the average of the left and right contact angle. Because SOCAL is a transparent coating, we were also able to confirm that droplets on the surfaces retained an axisymmetric shape during evaporation by conducting control experiments using the simultaneous side profile and bottom up views.

Data presented in this paper show typical curves for each RH obtained from the average of three repeated evaporations. The data for each RH was averaged into 100 equally spaced bins for each measured quantity (elapsed time, contact angle, contact radius). All of the experiments were carried out on five separately made SOCAL-treated glass slides at various locations on the slides. The different humidity experiments were carried out nonsequentially to ensure that no aging effects were observed.

DOI: 10.1021/acs.langmuir.8b03849
Langmuir 2019, 35, 2989−2996

3. EXPERIMENTAL RESULTS

3.1. Typical Evaporation Sequence. Figure 3 shows the contact angle θ, and contact area, πr^2, as a function of time during a typical

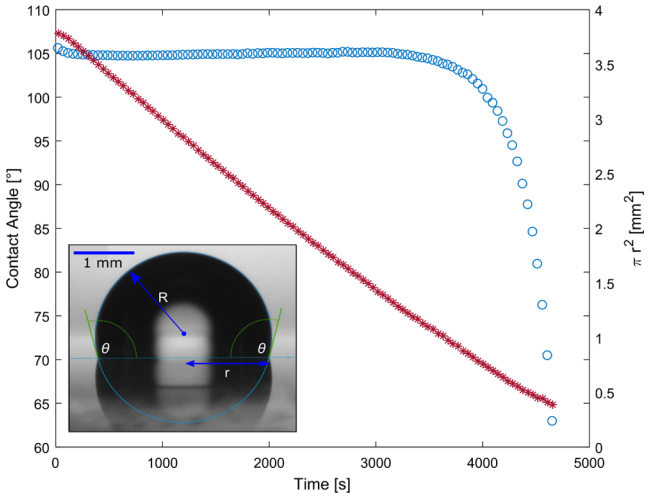

Figure 3. Typical evaporation showing the contact angle (ooo) and contact area (***) as a function of time. The conditions of this typical evaporation are a 4 μL droplet of DI water, 25 °C, and 70% RH. The inset shows the ellipse fitting of the droplet to measure the contact angle (θ), contact radius (r), and spherical radius (R).

sessile droplet evaporation sequence. After short initial relaxation, when a droplet is deposited, a CCA is observed for the majority of the evaporation time. During the CCA period, the contact area reduces linearly with time. The short initial relaxation is likely to be due to the droplet equilibrating to the surface, temperature, and RH (e.g., see McHale et al.[33]). The final stage of evaporation appears to be correlated to the observation of mineral deposit formation when the droplet radius reduced to ~0.5 mm, which is the radius at which the contact angle first begins to decrease.

3.2. Influence of RH. The CCA mode of evaporation occurs across a broad range of RH (10−70%). Figure 4 illustrates a typical evaporation at the lowest and highest values of RH. Even though these extremes in RH result in significantly different total evaporation times of 23 min and 2 h 15 min, the droplet evaporation sequences demonstrate the same behavior. The presence of the syringe (seen at the top of each image in Figure 4) illustrates that an evaporating droplet remains centered, close its initial deposition location, from the start to end of their evaporation. This provides confidence that the droplet contact line is completely mobile and free from pinning at all locations around the droplet.

Figure 5 shows a full set of sessile droplet evaporation sequences across the range of RH from 10 to 70% in steps of 10% and using the volume as the horizontal axis to collapse all the data onto a single plot. The central inset in Figure 5 reveals that the CCA during evaporation has two distinct values. The contact angle in the range of the RH of 10−30% is 101° while in the range of the RH of 30−40%, there is a

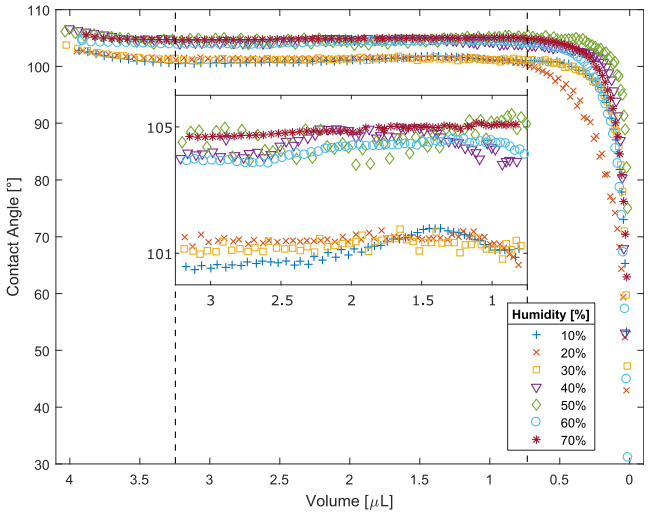

Figure 5. Contact angle as a function of volume. The dashed lines indicate the CCA mode of evaporation. The central inset is a magnification of the CCA mode evaporation, showing the two contact angles for low (10−30%) and high (40−70%) RH.

sharp rise in the CCA to 104.5°, which remains the value observed for the range from 40 to 70%. The step nature of this transition is further detailed in Figure 6, which presents data for the RH range 30−40%

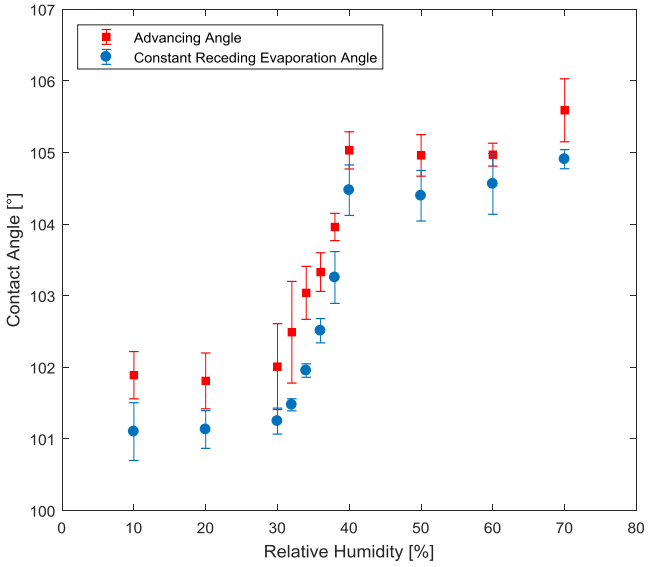

Figure 6. Step change in the value of the CCA for evaporation at different RH values.

using steps in the RH of 2%. Advancing angle measurements were carried out at each RH value to confirm the surface retained low

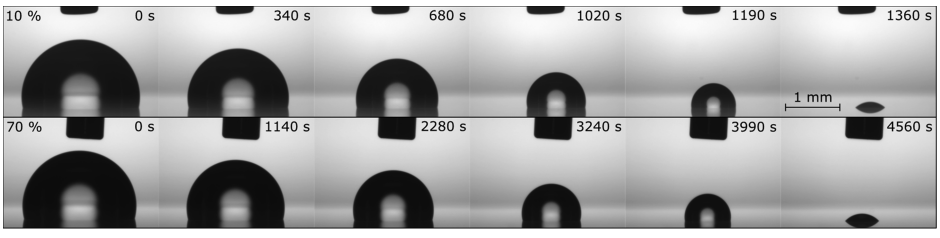

Figure 4. Evaporation time lapse at 10 and 70% RH. The syringe needle is kept in the image to show the droplets evaporate, moving radially inward in all directions.

DOI: 10.1021/acs.langmuir.8b03849
Langmuir 2019, 35, 2989−2996

contact-angle hysteresis despite this step change in the contact angle. Evaporation causes the contact line to retreat slower than a needle withdrawing liquid; therefore, the receding angle at a given RH is the angle observed during evaporation of liquid at that RH. Contact-angle hysteresis estimated using the constant receding angle during evaporation and the measured advancing contact angle prior to evaporation was largest at RH = 34% with $\Delta\theta_{CAH} = (1.09 \pm 0.27)°$ and lowest at RH = 60% with $\Delta\theta_{CAH} = (0.41 \pm 0.16°)$. Figure 6 shows $\Delta\theta_{CAH}$ remains low for both contact angle regimes with $\Delta\theta_{CAH} < 2°$.

4. ANALYSIS AND DISCUSSION

We first focus on the qualitative features of typical evaporation sequences. After a droplet is deposited, there is an immediate and short duration initial relaxation of the contact angle. The decrease in the contact angle could be due to changes in temperature as evaporation establishes itself and evaporative cooling of the droplet and substrate occurs. For isolated evaporating spherical drops, the cooling is determined by the evaporation rate,[34] and this will also occur for sessile droplets with the evaporative cooling correlated to the RH, which controls the rate of evaporation. In addition, thermal properties of the substrate will influence how effectively thermal energy can be supplied to maintain the temperature of the substrate surface. For example, Sefiane et al. show a link between the cooling effect on a droplet and the thermal properties of the substrate.[35] A further possibility is that evaporation creates a local RH which, given the contact angle is over 90°, may be important for the precise value of the contact angle because of the confined wedge space defined by the droplet and the substrate near the contact line. The simplest interpretation is that, although the contact-angle hysteresis is very small, an evaporating droplet is simply adopting a receding contact angle, which is slightly lower (1−2°) than its initial value on deposition.

The initial relaxation is then followed by a CCA period that dominates the overall evaporation time. An unexpected feature in our data is the apparent separation into two distinct values of the CCA of 101° and 104.5° for this CCA evaporation mode. This step change for RH between 30 and 40% is shown in Figure 6 and is reminiscent of the shape of a type V adsorption isotherm.[36] These two contact angle values can be compared to the 0.6° increase in contact-angle hysteresis at the lower RH values quantified using measurements via addition and withdrawal of liquid to a droplet. We excluded the step change being a consequence of a dynamic contact angle, defined by the speed of retreat of the contact line, by conducting receding contact-angle measurement by withdrawal of liquid at different rates. We can also consider possible origins of the step change using Young's law (eq 1), for which there are two interfacial tensions, γ_{LV} and γ_{SV}, that depend on the vapor. The first of these, the surface tension γ_{LV}, is known from pendant drop measurements to have a smooth change with temperature and RH over the range used in our experiments (72.2−75.5 mN m^{-1}).[37,38] However, the second of these, the solid−vapor interfacial tension γ_{SV}, is a candidate for the origin of a step change in the observed contact angle. This might occur if a film of vapor condensed on the solid over the narrow 30−40% range of RH, thereby replacing the solid−vapor interface by solid−liquid and liquid−vapor interfaces. To consider this possibility, we attempted to measure mass change on a SOCAL-coated glass surface using a dynamic vapor sorption (DVS) method, but unfortunately, it was not possible to obtain reliable results because of the small relative changes in mass. We also visually observed changes in reflectivity with RH changes using a glass surface which had half of its area treated with the SOCAL coating but did not observe any change indicating condensation had occurred. Another possibility is that the solid−vapor interfacial tension changes because of the adsorption of a monolayer of vapor. This could cause an increase in the contact angle as the RH increases, as observed experimentally, because of increased cohesion of the water molecules and, hence, a decrease in the solid−vapor interfacial tension γ_{SV}. A further possibility is that adsorption of a monolayer of water vapor could cause a step change in the mobility of the PDMS chains in the SOCAL coating for RH above and below the 30−40% range. From these possibilities, vapor adsorption appears to be the most likely reason for the step change in the contact angle with increasing RH.

In the very final stages of evaporation, the contact angle reduces rapidly and after the droplet had completely evaporated, we observed deposits were present over an area corresponding to that at which the contact angle first began to reduce. We therefore verified that the water we used did not contain solid particles. Energy-dispersive X-ray spectroscopy and scanning electron microscopy analysis of these deposits showed them to be composed of NaCl, AlCl, MgCl, and KCl. This suggests trace amounts of salts precipitated out of water at a volume of 0.6 ± 0.1 μL, and their deposition on the SOCAL-coated glass surface then created a self-pinning effect.

We now focus on a quantitative analysis of the evaporation sequences. Consider a sphere of liquid suspended in air far from any surface for which the rate of change in its volume due to diffusion-limited evaporation is given by

$$\frac{dV}{dt} = \frac{4\pi R D \Delta c}{\rho} \tag{2}$$

where V is volume, R is the spherical radius of the droplet, D is the diffusion coefficient of water vapor in air, Δc is the difference between the vapor concentration close to the droplet and far away ($\Delta c = c_0 - c_\infty$), and ρ is the density of the liquid. Here, the rate of change of volume arises from the net flux at the liquid−vapor interface integrated over the free surface of the droplet as discussed in the review by Cazabat and Guéna.[12] The same droplet resting on a solid surface will adopt a spherical cap shape, provided it is smaller than the capillary length, which for water is κ^{-1} = 2.73 mm, and its contact area is not prevented by contact-line pinning from adopting a circular shape. Geometrically, this shape is defined by its contact angle, θ, with the surface and a contact radius r, as illustrated in the inset to Figure 3. Knowing these two parameters enables the volume of a spherical cap to be calculated using

$$V = \frac{\pi}{3}\frac{(\cos\theta - 1)^2(2 + \cos\theta)r^3}{\sin^3\theta} \tag{3}$$

Other geometrical parameters, such as the spherical radius, R, can also be calculated

$$R = \left(\frac{3V}{\pi(2 - 3\cos\theta + \cos^3\theta)}\right)^{1/3} \tag{4}$$

In addition to the change in the droplet geometry from spherical to spherical cap, diffusion-limited evaporation is also influenced by the change in space into which vapor can diffuse. Thus, a completely spherical droplet with a contact angle of

DOI: 10.1021/acs.langmuir.8b03849
Langmuir 2019, 35, 2989−2996

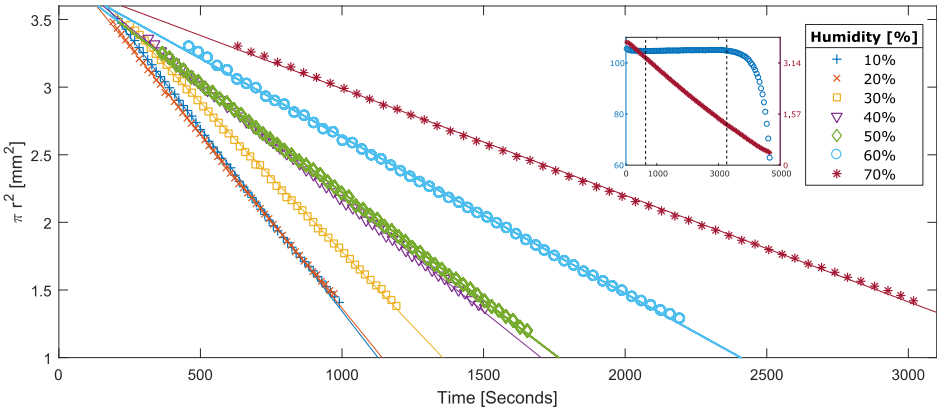

Figure 7. Contact area πr^2 as a function of time for evaporations at RH 10−70%. The line through each data set represents the linear fit used to calculate D_{RH}. The inset shows the representative contact angle and contact area as a function of time, where the data between the dashed lines show the section of the evaporation that is the CCA mode.

180° just touching in the flat solid surface does not evaporate as fast as a spherical droplet far from the surface. Picknett and Bexon considered sessile droplet evaporation and provided an exact closed-form solution for its diffusion-limited evaporation, which has a similar form to eq 2 but with an additional factor, $f(\theta)$, which is a function of the contact angle

$$\frac{dV}{dt} = \frac{4\pi RD\Delta c}{\rho} f(\theta) \tag{5}$$

To aid numerical calculations, they provided polynomial fits to $f(\theta)$, covering the full contact-angle range. For our experiments, the appropriate polynomial fit is for angles between $10° < \theta < 180°$ and is

$$f_{PB}(\theta) = \frac{1}{2}(0.00008957 + 0.6333\theta + 0.116\theta^2 - 0.8878\theta^3 + 0.01033\theta^4) \tag{6}$$

where θ is in radians. Because the droplets in our experiments conform to spherical caps, and unlike the work of Guan et al. on SLIPS[28] there is no wetting ridge present, these equations can be used directly to analyze our data. For the CCA mode with side profile observations providing both contact angle and contact radius, the most appropriate equation arises by substituting eq 3 into eq 5 to give

$$\frac{d(\pi r^2)}{dt} = \frac{8\pi D\Delta c \sin^2\theta f_{PB}(\theta)}{\rho(\cos\theta - 1)^2(2 + \cos\theta)} \tag{7}$$

As the right-hand side of eq 7 does not depend on time for the CCA mode of evaporation, the contact area should reduce linearly with time.

Figure 7 shows representative data for sessile droplet evaporation on our SOCAL surfaces for each value of RH (10−70%) and each can be seen to provide excellent agreement with a linear fit; the inset in Figure 7 illustrates the time range used to define the CCA range. From the slopes in Figure 7, the diffusion coefficient for each RH, D_{RH}, has been calculated using eq 6 and is shown in Table 1. These values of D_{RH} range from 2.31×10^{-5} to 2.87×10^{-5} m^2 s^{-1} with an average of $(2.58 \pm 0.20) \times 10^{-5}$ m^2 s^{-1}, which compares well to the literature value of 2.48×10^{-5} m^2 s^{-1}.[39]

Figure 7 provides confidence that we have observed CCA mode evaporation, which is diffusion-limited, and Table 1 confirms that the extracted diffusion coefficients from each RH

Table 1. Calculated Diffusion Coefficient for Each RH Compared to the Literature Value

RH [%]	$d\pi r^2/dt$ [mm^2 s^{-1}]	D_{RH} [$\times 10^{-5}$ m^2 s^{-1}]	D literature [$\times 10^{-5}$ m^2 s^{-1}]
10	−0.002699	2.47	2.48
20	−0.002513	2.58	2.48
30	−0.002202	2.58	2.48
40	−0.001678	2.44	2.48
50	−0.001640	2.87	2.48
60	−0.001297	2.82	2.48
70	−0.000754	2.31	2.48
	average	**2.58 ± 0.20**	**2.48**

are consistent with the literature values. However, because the diffusion coefficient should not depend on the RH, rearranging eq 7 and relating the RH to vapor concentration by $\Delta c = c_0((RH/100) - 1)$, allows a single estimated diffusion coefficient, D_E, to be calculated using all experiments across the range of RH 10−70%

$$\frac{\rho(\cos\theta - 1)^2(2 + \cos\theta)}{8\pi\Delta c \sin^2\theta f_{PB}(\theta)} \frac{d(\pi r^2)}{dt} = D_E\left(\frac{RH}{100} - 1\right) \tag{8}$$

Figure 8 shows data from Figure 7 plotted using eq 8, and the gradient from this gives an estimate of the diffusion coefficient of $D_E = (2.44 \pm 0.48) \times 10^{-5}$ m^2 s^{-1}, which is an improved estimate compared to the single RH estimates and which is within 2% of the literature value.

Finally, because Wang and McCarthy have reported that SOCAL surfaces are omniphobic and have low contact-angle hysteresis to a wide range of liquids, including diiodomethane, toluene, hexadecane, cyclohexane, decane, and hexane,[29] the accuracy of our evaporation method of determining the diffusion coefficient for water suggests that a SOCAL-coated glass surface could be used to determine the diffusion coefficients for a wide range of other liquids.

5. CONCLUSIONS

In this work, we have shown it is possible to observe the CCA evaporation mode on a flat smooth (nontextured) solid surface by creating SOCAL-coated surfaces with extremely low contact-angle hysteresis. This differs from previous attempts to observe the CCA mode, which have relied on the use of

DOI: 10.1021/acs.langmuir.8b03849
Langmuir 2019, 35, 2989−2996

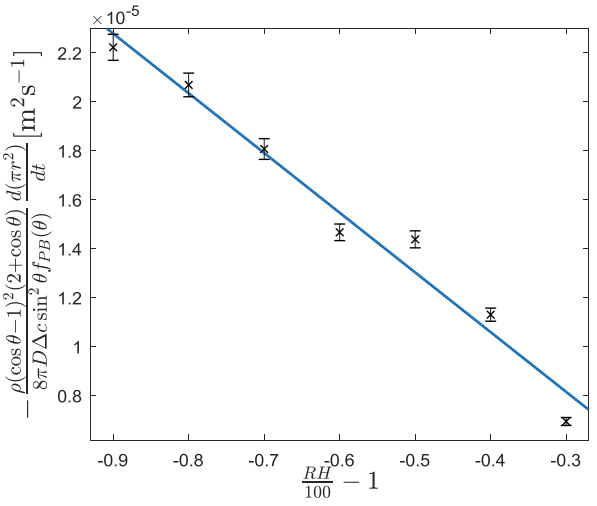

Figure 8. $d\pi r^2/dt$ as a function of RH. The gradient of the plot gives the calculated diffusion coefficient D_E.

textured solid surfaces, or a lubricant oil that removes all contacts with a solid surface. We have also observed a step change in the CCA value occurring in a narrow range of RH (30−40%), which is indicative of the adsorption of water vapor on the surface and reminiscent of a type V isotherm. The value of the CCA during evaporation has been shown to be consistent with the ideal contact angle from Young's law estimated by using independent measurements of the advancing and receding contact angle. Quantitative analysis of the sessile droplet evaporation sequences provides accurate measurements of the diffusion constant of the evaporating liquid. Hence, this methodology can provide a simple and reliable way to characterize the volatility of a wide range of other liquids.

AUTHOR INFORMATION

Corresponding Author

*E-mail: glen.mchale@northumbria.ac.uk.

ORCID

Steven Armstrong: 0000-0002-0520-8498
Glen McHale: 0000-0002-8519-7986
Rodrigo Ledesma-Aguilar: 0000-0001-8714-0556

Notes

The authors declare no competing financial interest.

ACKNOWLEDGMENTS

The authors gratefully acknowledge Professor Chris Hardacre and Huan Xiang from the School of Chemical Engineering & Analytical Science, University of Manchester, for assistance with DVS measurements and discussion of the results and Professor Doris Vollmer (Max Planck Institute for Polymer Research, Mainz) for discussion on the SOCAL method. R.L.-A. acknowledges support from EPSRC (grant no. EP/P024408/1). S.A. would also like to acknowledge Dr. G. Launay, Dr. E. Ruiz-Gutierrez, Dr. P. Agrawal and H. Barrio-Zhang for valuable advice and technicals support. S.A. would also like to acknowledge Northumbria University at Newcastle for financial support.

REFERENCES

(1) Erbil, H. Y. Evaporation of Pure Liquid Sessile and Spherical Suspended Drops: A Review. *Adv. Colloid Interface Sci.* **2012**, *170*, 67−86.
(2) Lim, T.; Han, S.; Chung, J.; Chung, J. T.; Ko, S.; Grigoropoulos, C. P. Experimental Study on Spreading and Evaporation of Inkjet Printed Pico-Liter Droplet on a Heated Substrate. *Int. J. Heat Mass Transf.* **2009**, *52*, 431−441.
(3) Li, T.; Xu, M.; Hung, D.; Wu, S.; Cheng, S. Understanding the Effects of Fuel Type and Injection Conditions on Spray Evaporation Using Optical Diagnostics. *2015 SAE World Congress and Exhibition*; SAE Technical Paper Series, 2015 April (March).
(4) Yuen, M. C.; Chen, L. W. Heat-Transfer Measurements of Evaporating Liquid Droplets. *Int. J. Heat Mass Transf.* **1978**, *21*, 537−542.
(5) Deegan, R. D.; Bakajin, O.; Dupont, T. F.; Huber, G.; Nagel, S. R.; Witten, T. A. Capillary Flow as the Cause of Ring Stains from Dried Liquid Drops. *Nature* **1997**, *389*, 827−829.
(6) McHale, G. Surface Free Energy and Microarray Deposition Technology. *Analyst* **2007**, *132*, 192−195.
(7) Frommelt, T.; Kostur, M.; Wenzel-Schäfer, M.; Talkner, P.; Hänggi, P.; Wixforth, A. Microfluidic Mixing via Acoustically Driven Chaotic Advection. *Phys. Rev. Lett.* **2008**, *100*, 034502.
(8) Eral, H. B.; Augustine, D. M.; Duits, M. H. G.; Mugele, F. Suppressing the Coffee Stain Effect: How to Control Colloidal Self-Assembly in Evaporating Drops Using Electrowetting. *Soft Matter* **2011**, *7*, 4954−4958.
(9) Young, T. III. An Essay on the Cohesion of Fluids. *Philos. Trans. R. Soc. London* **1805**, *95*, 65−87.
(10) Picknett, R. G.; Bexon, R. The Evaporation of Sessile or Pendant Drops in Still Air. *J. Colloid Interface Sci.* **1977**, *61*, 336−350.
(11) Stauber, J. M.; Wilson, S. K.; Duffy, B. R.; Sefiane, K. On the Lifetimes of Evaporating Droplets with Related Initial and Receding Contact Angles. *Phys. Fluids* **2015**, *27*, 122101.
(12) Cazabat, A.-M.; Guéna, G. Evaporation of Macroscopic Sessile Droplets. *Soft Matter* **2010**, *6*, 2591.
(13) Larson, R. G. Transport and Deposition Patterns in Drying Sessile Droplets. *AIChE J.* **2014**, *60*, 1538−1571.
(14) Wong, T.-S.; Kang, S. H.; Tang, S. K. Y.; Smythe, E. J.; Hatton, B. D.; Grinthal, A.; Aizenberg, J. Bioinspired Self-Repairing Slippery Surfaces with Pressure-Stable Omniphobicity. *Nature* **2011**, *477*, 443−447.
(15) Smith, J. D.; Dhiman, R.; Anand, S.; Reza-Garduno, E.; Cohen, R. E.; McKinley, G. H.; Varanasi, K. K. Droplet Mobility on Lubricant-Impregnated Surfaces. *Soft Matter* **2013**, *9*, 1772−1780.
(16) Cassie, A. B. D.; Baxter, S. Wettability of Porous Surfaces. *Trans. Faraday Soc.* **1944**, *40*, 546.
(17) Onda, T.; Shibuichi, S.; Satoh, N.; Tsujii, K. Super-Water-Repellent Fractal Surfaces. *Langmuir* **1996**, *12*, 2125−2127.
(18) Barthlott, W.; Neinhuis, C. Purity of the Sacred Lotus, or Escape from Contamination in Biological Surfaces. *Planta* **1997**, *202*, 1−8.
(19) Shirtcliffe, N. J.; McHale, G.; Atherton, S.; Newton, M. I. An Introduction to Superhydrophobicity. *Adv. Colloid Interface Sci.* **2010**, *161*, 124−138.
(20) McHale, G.; Aqil, S.; Shirtcliffe, N. J.; Newton, M. I.; Erbil, H. Y. Analysis of Droplet Evaporation on a Superhydrophobic Surface. *Langmuir* **2005**, *21*, 11053−11060.
(21) Wenzel, R. N. Resistance of Solid Surfaces to Wetting by Water. *Ind. Eng. Chem.* **1936**, *28*, 988−994.
(22) Zhang, X.; Tan, S.; Zhao, N.; Guo, X.; Zhang, X.; Zhang, Y.; Xu, J. Evaporation of Sessile Water Droplets on Superhydrophobic Natural Lotus and Biomimetic Polymer Surfaces. *ChemPhysChem* **2006**, *7*, 2067−2070.
(23) McLauchlin, M. L.; Yang, D.; Aella, P.; Garcia, A. A.; Picraux, S. T.; Hayes, M. A. Evaporative Properties and Pinning Strength of Laser-Ablated, Hydrophilic Sites on Lotus-Leaf-Like, Nanostructured Surfaces. *Langmuir* **2007**, *23*, 4871−4877.

DOI: 10.1021/acs.langmuir.8b03849
Langmuir 2019, 35, 2989−2996

(24) Tan, S.-x.; Zhang, X.-y.; Zhao, N.; Xu, J. Simulation of Sessile Water-Droplet Evaporation on Superhydrophobic Polymer Surfaces. *Chin. J. Chem. Phys.* **2007**, *20*, 140−144.
(25) Jung, Y. C.; Bhushan, B. Wetting Behaviour during Evaporation and Condensation of Water Microdroplets on Superhydrophobic Patterned Surfaces. *J. Microsc.* **2008**, *229*, 127−140.
(26) Kulinich, S. A.; Farzaneh, M. Effect of Contact Angle Hysteresis on Water Droplet Evaporation from Super-Hydrophobic Surfaces. *Appl. Surf. Sci.* **2009**, *255*, 4056−4060.
(27) Gelderblom, H.; Marín, Á. G.; Nair, H.; van Houselt, A.; Lefferts, L.; Snoeijer, J. H.; Lohse, D. How Water Droplets Evaporate on a Superhydrophobic Substrate. *Phys. Rev. E: Stat., Nonlinear, Soft Matter Phys.* **2011**, *83*, 026306.
(28) Guan, J. H.; Wells, G. G.; Xu, B.; McHale, G.; Wood, D.; Martin, J.; Stuart-Cole, S. Evaporation of Sessile Droplets on Slippery Liquid-Infused Porous Surfaces (SLIPS). *Langmuir* **2015**, *31*, 11781−11789.
(29) Wang, L.; McCarthy, T. J. Covalently Attached Liquids: Instant Omniphobic Surfaces with Unprecedented Repellency. *Angew. Chem., Int. Ed.* **2015**, *55*, 244−248.
(30) Jin, Y.; Zhang, L.; Wang, P. Atmospheric Water Harvesting: Role of Surface Wettability and Edge Effect. *Glob. Challenges* **2017**, *1*, 1700019.
(31) Mizutani, T.; Enomoto, T.; Satake, U. Surgical diamond wheels for minimally invasive surgery in bone resection under saline supply. *Precis. Eng.* **2018**, *77*, 243−246.
(32) Daniel, D.; Timonen, J. V. I.; Li, R.; Velling, S. J.; Kreder, M. J.; Tetreault, A.; Aizenberg, J. Origins of Extreme Liquid Repellency on Structured, Flat, and Lubricated Hydrophobic Surfaces. *Phys. Rev. Lett.* **2018**, *120*, 244503.
(33) McHale, G.; Rowan, S. M.; Newton, M. I.; Banerjee, M. K. Evaporation and the Wetting of a Low-Energy Solid Surface. *J. Phys. Chem. B* **1998**, *102*, 1964−1967.
(34) Erbil, H. Y.; Dogan, M. Determination of Diffusion Coefficient−Vapor Pressure Product of Some Liquids from Hanging Drop Evaporation. *Langmuir* **2000**, *16*, 9267−9273.
(35) David, S.; Sefiane, K.; Tadrist, L. Experimental Investigation of the Effect of Thermal Properties of the Substrate in the Wetting and Evaporation of Sessile Drops. *Colloids Surf., A* **2007**, *298*, 108−114.
(36) Sing, K. S. W. Reporting Physisorption Data for Gas/solid Systems with Special Reference to the Determination of Surface Area and Porosity (Recommendations 1984). *Pure Appl. Chem.* **1985**, *57*, 603−619.
(37) Pérez-Díaz, J. L.; Álvarez-Valenzuela, M. A.; García-Prada, J. C. The Effect of the Partial Pressure of Water Vapor on the Surface Tension of the Liquid Water-Air Interface. *J. Colloid Interface Sci.* **2012**, *381*, 180−182.
(38) Portuguez, E.; Alzina, A.; Michaud, P.; Oudjedi, M.; Smith, A. Evolution of a Water Pendant Droplet: Effect of Temperature and Relative Humidity. *Nat. Sci.* **2017**, *09*, 1−20.
(39) Lide, D. R. *CRC Handbook of Chemistry and Physics: A Ready Reference Book of Chemical and Physical Data*, 1992; Vol. *268*.

DOI: 10.1021/acs.langmuir.8b03849
Langmuir 2019, 35, 2989−2996